A general and adaptive synthesis protocol for high-quality organosilane selfassembled monolayers as tunable surface chemistry platforms for biochemical applications

Authors' post-prints

Artusio F., Fumagalli F., Bañuls-Ciscar J., Ceccone G., Pisano R.* (2020). A general and adaptive synthesis protocol for high-quality organosilane self-assembled monolayers as tunable surface chemistry platforms for biochemical applications. Biointerphases **15**(*4*):041005-1-12.

* Corresponding author: roberto.pisano@polito.it

A general and adaptive synthesis protocol for high-quality organosilane self-assembled monolayers as tunable surface chemistry platforms for biochemical applications

Fiora Artusio[1], Francesco Fumagalli[2], Jorge Bañuls-Ciscar[2], Giacomo Ceccone[2], Roberto Pisano[1]*

[1] Department of Applied Science and Technology, Politecnico di Torino, corso Duca degli Abruzzi 24, 10129, Torino, Italy

[2] European Commission, Directorate General Joint Research Centre, Directorate F – Health, Consumers and Reference Materials, Unit F.2 – Consumer Products Safety, Via E. Fermi 2749, TP125, I-21027 Ispra (VA), Italy

*Corresponding author, e-mail: roberto.pisano@polito.it, Tel. +39 011 0904679

Abstract

The controlled modification of surface properties represents a pervasive requirement to be fulfilled when developing new technologies. In this paper, we propose an easy-to-implement protocol for the functionalization of glass with Self-Assembled Monolayers (SAMs). The adaptivity of the synthesis route was demonstrated by the controlled anchoring of thiol, amino, glycidyloxy, and methacrylate groups onto the glass surface. The optimization of the synthetic pathway was mirrored by extremely smooth SAMs (approx. 150 pm roughness), layer thickness comparable to the theoretical molecule length, absence of silane islands along the surface, quasi-unitary degree of packing, and tailored wettability and charge. The functionalization kinetics of two model silanes, 3-mercapto- and 3-amino-propyltrimethoxysilane, was determined by cross-comparing X-Ray Photoelectron Spectroscopy (XPS) and Time of Flight Secondary Ion Mass Spectrometry (ToF-SIMS) data. Our SAMs with tailored physico-chemical attributes will be implemented as supports for the crystallization of pharmaceuticals and biomolecules in upcoming studies. Here, the application to a small molecule drug model, namely aspirin, was discussed as proof of concept.

Keywords: self-assembled monolayer (SAM), functionalization, surface analysis, kinetics, crystallization

Introduction

Surface functionalization using Self-Assembled Monolayers (SAMs) has been applied to different substrates and constitutes one of the most robust methods to chemically modify surfaces. Self-assembly is an autonomous process where the components of a system organize themselves in an ordered manner. Such a phenomenon naturally occurs at all scales (from nano to macro) being the fundamental growth step of hierarchical structures [1,2].

SAMs have been widely employed for bio-sensors [3,4], protein crystallization [5,6], engineering of organic thin films [7], and field-effect transistors [8,9] but also for designing smart surfaces [10], for improving tribological behavior of microelectromechanical systems [11], and for the functionalization of semiconductors

nanostructures [12]. As polymer brushes may be grown from SAMs, applications in optics, corrosion, adhesion, and material science have been reported [13,14]. Furthermore, graft polymerization on SAMs has been widely applied not only to flat substrates but also to nanoparticles or fibres [15].

Generally, SAMs synthesis involves a monomolecular surfactant film which spontaneously assembly on a surface because of the lowering of interfacial tension between two phases. Self-assembly and covalent bonding of molecules to a surface represent the result of a confinement strategy. More generally, 3-D confinement has allowed the synthesis of nanoparticles with different structures [16,17] or the tuning of a crystalline state of pharmaceutical products [18]. When confinement strategies are restricted to 2-D systems, the spontaneous assembly of selected building blocks leads to selective and ordered functionalization of pre-determined areas.

The two most popular methods for SAM synthesis involve the reaction between trialkoxy- or trichlorosilane and hydroxylated silicon, as well as between disulfide or thiol reactants and gold [19]. The chemistry of the surfactant and the intermolecular forces, instead, govern the degree of order of the layer [20]. Ranging from SAMs that resemble liquids because of their internal disorder to quasi-crystalline structures, one can play with a plethora of different surface chemistries and conformations. For example, in non-polar SAMs, the nanoscale structure of water interface molecules shows a correlation with the degree of order of the layer [21]. Also, it has been found that the ligand chain length, the nature and diameter of the core of gold nanoparticles can affect the SAM morphology [22].

In the literature, the protocols of SAM synthesis commonly involve either the vapor deposition [23,24] or the wet-chemistry route [25,26]. They substantially differ in the phase containing the monomer. In the former case, the monomer chemisorbs on a substrate from the vapor phase by increasing its partial pressure, while in the latter it directly comes from the solution. These latter techniques also include the drop-cast [27] and the direct heating of pristine silanes deposited onto the surface [28]. Many factors affect the quality of the functionalized surface, i.e., the functionalization density and reproducibility. These factors include the synthesis environment, the solvent, the chemistry of silanes, and the pretreatment/cleaning of the substrate. For example, the volume of water in the system strongly affects the monolayer formation and its ordering, both for shortage or excess conditions [29–32]. Furthermore, in the case of nanoparticles, several surface analysis studies have demonstrated that sample cleaning and purification may influence surface coverage, thus

affecting the reliability and reproducibility of the functionalization process [33,34]. Despite the large number of applications of this method of surface functionalization, the selection of appropriate conditions for the synthesis of a monolayer and controlled monomer anchoring is still under debate [35–39]. In this perspective, the comparison of results obtained through different protocols could be beneficial to the standardization of the SAM synthesis.

SAMs are often used as linkers for the anchoring of biomolecules, e.g., proteins and antibodies, nanoparticles, and other constructs [36]. For these applications, it is crucial to control the thickness and uniformity of the monomer layer, and the density of active groups exposed on the surface. These properties may change with the synthesis protocol, and their accurate control is rather difficult. Furthermore, the macro-characterization techniques, e.g., the contact angle measurement, cannot give a detailed description of the surface properties. The use of advanced micro-characterization techniques is, thus, required to assess the quality of the functionalization process. In this scenario, a wide variety of synthesis protocols for surface functionalization with alkoxysilanes is reported in literature, but studies are generally limited to just one or two functionalizing molecules [40–45]. Therefore, a generalized and robust protocol for the preparation of SAMs which could potentially be applied to any alkoxysilane is missing, along with the thorough physico-chemical characterization of the prepared SAMs.

This study presents a protocol for the synthesis of SAMs starting from trimethoxysilanes, which is fully compatible with the silane chemistry. The method ensures the precise control of surface functionalization with monolayers exposing thiol, amino, methacrylate, and glycidyloxy groups. To the best of our knowledge, this is the first work presenting and validating a single synthesis protocol to prepare SAMs from these four specific trimethoxysilanes. The proposed protocol could potentially be applied to any alkoxysilane since the selected head groups strongly differed for their polarity, hydrogen-bonding ability, and acid-base behavior. We have evaluated the impact of various synthesis parameters on the SAM surface characteristics, combining micro- and macro-characterization techniques. For example, we have investigated the influence of various silane head groups on the kinetics of SAM formation through X-ray Photoelectron Spectroscopy (XPS) and Time of Flight Secondary Ion Mass Spectrometry (ToF-SIMS). Other process parameters that have been studied include the type of solvent, the concentration of the functionalizing agent, and the operating temperature. We used various techniques to estimate the thickness of the functionalized layer, which

reasonably agreed with the thickness of a SAM. The fine-tuning of surface properties makes our SAMs ideal candidates for the control of pharmaceutical and biopharmaceutical crystallization [5]. As proof of concept, we studied the crystallization behavior of a small molecule drug, i.e., aspirin, in the presence of untreated glass, thiol- and amino-SAMs. SAMs were found to exert promoting or inhibiting actions over aspirin crystallization. The presented SAMs can also provide an ideal interface for the control of crystallization of more complex biomolecules, such as proteins.

Experimental methods

Materials

Borosilicate (D263M) glass coverslips were purchased from Neuvitro (Vancouver, USA). Hydrogen peroxide (30 wt% in water, ACS reagent), sulfuric acid (ACS reagent, assay 95.0 – 98.9%), acetone (ACS reagent, assay 99.5%), anhydrous toluene (< 0.001% water, assay 99.8%), toluene (ACS reagent, assay ≥ 99.5%), ethanol (puriss. p.a., absolute, assay ≥ 99.8%), 3-aminopropyltrimethoxysilane (APTMS, assay 97%), 3-glycidyloxypropyltrimethoxysilane (GPTMS, assay ≥ 98%), 3-mercaptopropyltrimethoxysilane (MPTMS, assay 95%), 3-(trimethoxysilyl)propylmethacrylate (TMSPM, assay 98%), water (HPLC grade), and aspirin (ASA, USP grade) were purchased from Sigma-Aldrich (Cesano Maderno -MI-, Italy). All the bottles of solvents used for the synthesis of SAMs were freshly opened.

Synthesis of SAMs on glass

Unless otherwise specified, all the operations concerning SAM synthesis were carried out at room temperature. Glass coverslips (diameter = 14 mm) were first sonicated twice in ethanol for 10 min (Bandelin, Sonorex, Germany) in order to remove coarse particles and contamination adsorbed on the surface. Then, coverslips were dried with nitrogen and incubated in a freshly prepared piranha solution (H_2SO_4:H_2O_2). 3:1 and 5:1 ratios were tested and immersion time was varied from 30 min to 2 h. Coverslips were then collected and thoroughly rinsed with deionized water. The pH of the rinsing water was monitored until the achievement of a neutral

value in order to remove any residue of the strongly oxidizing solution. The cleaned substrates were dried with nitrogen and then immediately dipped into the silane solutions. Various reaction media were tested, namely ethanol, acetone and anhydrous toluene. In the latter case, particular care was taken to carry out the withdrawal of solvent under nitrogen atmosphere to minimize water contamination. The silane concentration ranged from 0.014 M to 0.135 M. SAMs synthesis was carried out avoiding the use of glass for containers and instruments for manipulation so as to prevent the anchoring of the functionalizing agent onto the glassware walls. Silanization time varied between 15 min and 24 h, according to the considered reaction chemistry. Coverslips were then extracted and carefully rinsed with toluene, toluene: ethanol (1:1) and ethanol in order to remove any residue of solvents and unreacted species. Finally, blow-drying with nitrogen was performed. Few trials were dedicated to the investigation of SAM formation in a heated system. Activation and final rinsing were unaltered, whereas silanization was carried out for 4 h at 40 °C in a 0.054 M MPTMS solution. All the operations concerning the activation and the functionalization were performed under a fume-hood. In order to test the reproducibility of sample preparation, all samples were synthesized in triplicate by running distinct batches.

Physico-chemical characterization of SAMs

Contact angle

The effectiveness of piranha treatment and successive functionalization was assessed by static contact angle analyses (MSE DigiDrop, GBX, France). A 3 µL drop was produced thanks to a manual dispensing apparatus and placed on the treated surface. All the measurements were carried out using HPLC-grade water. Reproducibility was tested by analyzing three samples obtained from distinct batches prepared following the same synthesis protocol. For each sample, contact angle was measured on four different spots of the surface, so that the final contact angle value resulted from the average of 12 measurements.

Fourier Transformed InfraRed (FT-IR)

Fourier Transformed InfraRed in Attenuated Total Reflectance mode (FT-IR ATR, Nicolet iS50, Thermo Scientific, Waltham, MA, USA) was applied to prove the presence of -OH groups on piranha-treated glass. A

Smart ITX diamond was used for collecting FT-IR spectra between 600 and 4000 cm^{-1} with 4 cm^{-1} resolution. 64 scans per sample were run to obtain the final spectrum. Analyses were performed in triplicate.

155

Atomic Force Microscopy (AFM)

The surface topography was assessed *via* AFM (Solver NANO, NT-MDT Spectrum Instruments, Russia) in tapping mode. Scanned area was 1 x 1 μm^2 and each scan consisted of 256 lines. Cantilever frequency was 0.8 Hz and SiN_4 tips were used. Gwyddion software (ver. 2.51, Czech Metrology Institute) was used to process
160 the images after the analyses and calculate the average roughness (R_q) and the selected area difference (SAD). The analyses were performed in triplicate, and at least 3 measurements for each surface were carried out. A 5-order polynomial fit was applied to all the collected images.

Field Emission Scanning Electron Microscopy (FE-SEM)

165 Scanning electron microscopy (FE-SEM, Merlin, ZEISS, Germany) analyses were performed in triplicate in order to investigate the superficial morphology. The samples were metallized with a thin platinum layer to minimize the alteration of the substrates imaging due to the coating. The tip current was 100 pA, the operating voltage was set at 3 keV, and the working distance was 2.2 mm. An InLens detector was used.

170 *Ellipsometry*

Thin film thickness was evaluated by ellipsometry techniques (alpha-SE, J.A. Woollam Co., Lincoln, NE, USA). For all the measurements, 65°, 70° and 75° angles between incident light source and detector were used. Firstly, a model describing the intensity of light as a function of wavenumber has been developed for the untreated substrate using CompleteEASE software (ver. 4.63, J.A. Woollam Co.). Knowing the refractive
175 index (1.523), the thickness (0.15 mm) and the roughness (0.128 nm) of coverslips, a Cauchy model [46] has been implemented, and parameters such as complex refractive indexes and angle offsets for untreated glass were calculated by fitting experimental spectra. Then, for functionalized samples, layer thickness was calculated by setting the defined model for bare glass and fitting the refractive index and thickness of the additional Cauchy over layer. In every case, Mean Square Error (MSE) was below 2.5. Measurements were

carried out in triplicate and on three different spots per sample, in order to test sample and intra-batch uniformity.

Surface Zeta Potential (SZP)

Surface zeta potential was measured with a Dynamic Light Scattering-based technique (DLS, Zetasizer NANO ZS90, Malvern, Worcestershire, UK). SAM-functionalized coverslips were cut in pieces of about 4 × 6 mm^2 and attached onto a dedicated sample holder equipped with Pd electrodes. The sample was inserted into a disposable polystyrene cuvette filled with 1 mL of a standard microsphere latex acting as tracer. Tracer mobility was analyzed at different positions from the surface: 125, 250, 375, 500 and 1000 μm (the latter leading to the measurement of the zeta potential of the tracer itself). Analyses were performed on triplicates, and at least five measurements per sample were carried out.

X-Ray Photoelectron Spectroscopy (XPS)

The effective chemical functionalization of glass was explored by XPS (AXIS ULTRA, DLD Kratos Analytical, UK) equipped with a monochromatic Al Kα source (hν = 1486.6 eV) operating at 150 W. Wide scan spectra were recorded from 1100 to 0 eV binding energy in hybrid mode, "slot" aperture (400 x 700 μm^2 analysis area) and at 160 eV pass energy, whereas core level spectra were recorded using pass energy of 20 eV. The take-off angle (ToA), respect to the sample normal, was 0° for survey and high-resolution (HR) spectra, whilst angle-resolved XPS analyses (AR-XPS) were performed at ToA = 45° and 73°. Operating pressure was 6×10^{-7} Pa. Surface charging was compensated using low energy (~5 eV) electrons and adjusted using the charge balance plate on the instrument. Three different spots were analyzed for each sample. All the spectra were processed with CasaXPS (ver. 2.3.20). Spectra were calibrated setting hydrocarbon C1s at 285.0 eV. The surface composition was evaluated from the survey spectra, after a Tougaard U3-type background subtraction [47,48], using the relative sensitivity factors provided by the manufacturer. Peak fitting was performed with no preliminary smoothing. Symmetric Gaussian–Lorentzian (70% Gaussian and 30% Lorentzian) product functions were used to approximate the line shapes of the fitting components.

Time-of-Flight Secondary Ion Mass Spectrometry (ToF-SIMS)

ToF-SIMS (ToF IV, ION TOF GmbH, Germany) was also employed to characterize samples' chemistry. The accelerating voltage of the liquid metal ion gun (LMIG) was 25 keV, Bi_3^+ was employed as source of primary ions rastering over an area of 100 x 100 μm^2. The analyses were performed in static conditions keeping the ion dose below 10^{12} ions/cm^2. Acquisition time was 45 s, with a beam current of 0.5 pA and primary ion beam in pulsed mode. Positive mass spectra were collected while using an electron flood gun to dissipate surface charging. Spectra were collected on seven different spots per sample. CH^+, CH_2^+, CH_3^+, $C_2H_3^+$, CHO^+, $C_3H_4^+$, $C_3H_5^+$, $C_4H_7^+$ and $C_5H_9^+$ peaks were used to calibrate the positive spectra and a peak-list was created using the SurfaceLab software (ver. 6, IONTOF GmbH). Given the large number of peaks and spectra, Multivariate Analysis (MVA) methods were used to aid in the interpretation of the data by reducing the size of large data sets with a minimal loss of information [49–51]. The normalized intensities of all the peaks selected were loaded into the SimsMVA software [52]. Non-negative Matrix Factorialization (NMF) and Principal Component Analyses (PCA) were performed, providing endmembers in the case of NMF and principal components in the case of PCA. Scores and loadings are the typical outcome of PCA and NMF analyses. The scores describe the relationship between samples for each principal component/endmember, whereas the loadings provide information regarding how the variables (peak intensities) relate to each principal component/endmember [53,54].

Crystallization of aspirin on SAMs

Aspirin was dissolved in 38/62 (v/v) ethanol/water to achieve a supersaturation equal to 1.8 considering 15 °C as crystallization temperature. The crystallization experiments were carried out in multi-well plates. One surface was placed at the bottom of each well and then the 0.22 µm filtered ASA solution was pipetted on top. The plates were then sealed and placed inside an in-house incubator under a stereomicroscope (M125C, Leica Microsystems, Germany) for the continuous and automated monitoring of the samples. The temperature was set at 15 °C and 48 wells were monitored during each trial.

Results and discussion

A typical SAM wet synthesis is composed of three steps: substrate activation, SAM formation and final rinsing. Each step is crucial for the achievement of high-quality layers in terms of functionalization density, uniformity and reproducibility. Here, the effect of different functionalizing agents chemistries and synthesis parameters on the outcome of monolayer formation was investigated. Results emerged from macro and micro-characterization are presented.

Proper surface activation generates active sites on glass surface for the bonding of silane molecules. The coverage of the surface with hydroxyl groups enables the successive condensation reactions with silanes methoxy groups. Inhomogeneous or non-optimized surface activation would lead to localized deposits of silane molecules, resulting in non-uniform and incomplete layers. Surface hydroxylation was achieved by immersion in piranha solution. 3:1 and 5:1 ratios between sulfuric acid and hydrogen peroxide were tested. Immersion time ranged between 30 min and 2 h. The water contact angle of untreated glass was 62.9 (+/- 5.4)°. For all the tested conditions, the surface was found to be markedly more hydrophilic after exposure to piranha solution. More specifically, the increase in incubation time resulted to be beneficial for the decrease in the hydrophobicity of the glass. On one hand, 30 min were not enough for the effective removal of contaminants, especially for solutions containing less H_2O_2. On the other hand, longer incubation times favored the reproducibility of the surface treatment, as highlighted by lower standard deviations. 5:1 ratio and 1 h as incubation time was found to be the best combination for achieving extremely hydrophilic surfaces, i.e., contact angle < 2°, and unaltered topography, as reported in Tables 1 and S1, respectively. The more aggressive oxidizing solution allows the achievement of extremely hydrophilic surfaces in 1 h, minimizing the time devoted to preliminary activation treatments.

Table 1. Static contact angle of glass and relative standard deviation (Std Dev) as measured with HPLC water as probing liquid for different piranha ratios and hydroxylation times.

H_2SO_4 : H_2O_2 ratio	***Time, h***	***Contact angle, °***	***Std Dev, °***

3 : 1	0.5	9.6	1.8
3 : 1	1	6.1	3.3
3 : 1	2	7.2	1.7
5 : 1	0.5	17.1	6.7
5 : 1	1	< 2	
5 : 1	2	< 2	

The effectiveness of the piranha treatment in removing superficial organic contamination was assessed by XPS surveys, as depicted in Figure 1. The characteristic spectrum of untreated borosilicate glass showed strong O1s and Si2p peaks. The C1s peak observed on untreated samples was related to superficial hydrocarbon contamination. After the incubation in piranha solution, the atomic percentage of carbon was more than halved, decreasing from 19% down to about 8% (Table S2). The structure and the chemical composition of the bulk glass was not altered by the treatment. As shown in Table 2, the O/Si ratio, before and after piranha, was unaltered. Moreover, we analyzed the C1s region of glass by HR-XPS. As can be seen in Figure S1 and Table S3, a strong decrease in the C-C component was observed, along with an increase of almost three times in K2p atomic composition. This result proved the reduction of the thickness of contaminants layer since potassium can only be found in the bulk glass. Other elements like zinc, aluminium and titanium had also been detected in XPS surveys, as they are present as oxides impurities in the glass. However, their overall at% was below 3% as illustrated in Table S2, where the atomic compositions of all the samples are reported. Moreover, the presence of hydroxyl groups on the surface was confirmed by ATR FT-IR analyses, showing the typical broad shoulder of surface bonded -OH groups extending from 3200 cm^{-1} to 3600 cm^{-1}, as shown in Figure S2. The shoulder was detectable only in the piranha-treated samples, confirming that the signal was not only due to adsorbed water molecules from the atmosphere.

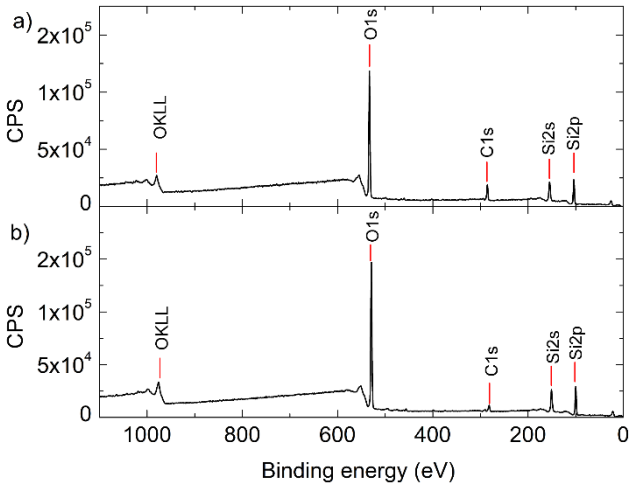

Figure 1. XPS surveys of (a) untreated and (b) piranha-cleaned glass recorded at ToA = 0 °. The peaks typical of bulk elements of borosilicate glass are highlighted. Atomic compositions are detailed in Table S2.

Once the effectiveness of the surface activation process has been demonstrated, the anchoring of various functionalizing agents onto the activated surfaces was studied. Firstly, 3-mercaptopropyltrimethoxysilane was designated as model molecule in order to optimize the synthesis conditions. Particular attention was devoted to the selection of the solvent employed as reaction medium. Ethanol, acetone and anhydrous toluene were tested. For the experiments, the incubation time was 15 h and the concentration of silane was 0.054 M. The effectiveness of the synthesis of the functionalized surface was first tested upon its superficial composition by XPS investigation. The analyses pointed out major differences among the samples as illustrated in Table 2, reporting the characteristic element ratios. Among all the elements detected, only sulfur was peculiar to the organic layer, whereas silicon and oxygen may refer either to bulk glass or to unreacted methoxy groups of the silanes. As regards carbon, the main contribution was due to the introduction of the propylic chain, but superficial contamination could not have been excluded. For the piranha-cleaned substrate, C/Si and O/Si were 0.32 and 2.57 respectively. Such ratios were found to decrease in all the samples undergoing a silanization treatment. However, the S/C ratio showed that the reaction medium plays a fundamental role on the synthesis outcome. Theoretically, the ideal S/C ratio is equal to 0.33, as one sulfur atom and three carbon atoms are present per MPMTS molecule. It can be seen that surfaces prepared using ethanol resulted in the farthest condition from the ideal ratio, followed by acetone. On the other hand, anhydrous toluene led to ratios closer to the desired ones, and the discrepancy between the ideal and the actual

S/C ratio was attributed to adventitious carbon contamination on the surface. These evidences were corroborated by contact angle measurements, showing a markedly less hydrophobic behavior for ethanol and acetone-based samples (water contact angle less than 40°). Conversely, the contact angle was 65.7° when anhydrous toluene was employed, confirming the anchoring of organic hydrophobic matter on the surface (see Table 2). Polar solvents were therefore found to be deleterious for getting high-quality thiol-terminated SAMs, as they may contain large amounts of water which, in turn, would favor intra-silanes polymerization at the expense of proper surface anchoring. Such an effect is emphasized when a polar protic solvent such as ethanol is employed: the number of -OH groups of the solvent by far exceeds that of the hydroxylated surface, masking the surface contribution to the condensation reaction. This may result in areas characterized by different amounts of anchored silanes or local deposits, as confirmed by the high standard deviation values of contact angle for these samples.

Table 2. Water contact angle (standard deviation in brackets) and characteristic element ratios (S/Si, C/Si, O/Si and S/C) as evaluated from XPS surveys (ToA = 0°). Data refer to untreated and piranha-cleaned glass and thiol-functionalized surfaces obtained with different sets of synthesis conditions. Solvent study involved ethanol, acetone and anhydrous toluene. Silane concentration study involved anhydrous toluene as reaction medium and concentration range from 0.054 to 0.135 M.

Solvent	***Concentration, M***	***Contact angle, °***	***S/Si***	***C/Si***	***O/Si***	***S/C***
Untreated glass		62.9 (5.4)	-	0.87	2.54	-
Piranha-cleaned glass		< 2	-	0.32	2.57	-
Ethanol	0.054	38.9 (4.9)	0.03	0.59	2.72	0.04
Acetone	0.054	33.4 (2.2)	0.06	0.58	2.80	0.10
Toluene (an.)	0.054	65.7 (1.7)	0.14	0.82	2.60	0.17

Toluene (an.)	0.027	63.2 (1.5)	0.15	1.47	2.37	0.10
Toluene (an.)	0.135	70.5 (2.1)	0.34	2.18	2.20	0.16
Toluene (an.) T = 40 °C t = 4 h	0.054	73.7 (3.5)	0.02	0.64	3.01	0.03

The presence of characteristic elements, i.e., sulfur and carbon, on the surface and their chemical state were investigated by XPS for the toluene-based sample. Successful functionalization was firstly confirmed by XPS survey scans, as reported in Figure 2 (a). The comparison with the survey spectrum of piranha-cleaned glass evidenced the presence of sulfur related peaks, S2s (~230 eV) and S2p (~ 164 eV), and the increase of C1s concentration, because of the addition of the propylic chain on the surface. The expected stoichiometry of unbound and bound silane molecules is reported in Table S4. The ideal composition of bound MPTMS and the actual composition of the sample, reported in Table S2, were first compared. The presence of a strong excess in silicon and oxygen denoted a significative contribution of glass elements to the overall signal. Such a finding corroborated the hypothesis of functionalization occurring in an extremely thin layer; further details will be provided later on. Also, taking into account carbon deriving from surface contamination, the residual carbon was related to the propylic chains of SAM. HR-XPS of C1s, reported in Figure 2 (b), evidenced two components: a major one at 285.0 eV related to the SAM hydrocarbon chain and a minor one at 286.5 eV attributable to C-O bonds [55]. The latter has been related to the presence of some residual unreacted methoxy groups of silanes. During progressive surface coating and consequent decay of hydroxylation, it is increasingly difficult for such groups to act as exit groups and participate to the condensation reaction. Nevertheless, the ideal anchoring of silanes to the glass surface by means of three covalent bonds is not feasible because of energetical issues. Bond strain limit the actual number of bonds to just one or two, and MPTMS cross-polymerization was supposed to contribute to the layer stability [56]. Also, the incomplete conversion of MPTMS could be ascribed to the presence of adsorbed or embedded silane molecules in the organic overlayer after the rinsing step. Moreover, C1s region shows two other minor peaks attributed to the K2p doublet. Additional AR-HR-XPS analyses were carried out in order to confirm the confinement of MPTMS to the very superficial layers of glass. As potassium is present exclusively in the glass substrate, it can be used as reference to assess the confinement of functionalization to the upper layers of the sample. As can be seen in Figure 2 (c),

increasing ToA led to an increase in C1s relative at% and a correspondent decrease in K2p at%. At 73°, K2p signal was barely detected since, in this configuration, the quantity of collected photoelectrons coming from the bulk of the sample is strongly reduced, favoring those coming from the surface of the sample. As regards sulfur, HR-XPS in Figure 2 (d) revealed the typical main peak splitting of metal ions at 162.8 and 164.1 eV, with the minor one being half of the major one. The $S2p_{ox}$ component at 168.4 eV was 13.8%, indicating a partial oxidation of the SAMs head groups [55].

XPS analyses represent a useful tool to demonstrate the confinement of functionalization within very few layers on the surface [57–61]. In order to estimate the number of layers of silane molecules attached onto the surface, the organic film thickness was calculated starting from XPS data. Two models based on the Electronic Attenuation Length (EAL) and the thickogram approaches were considered [62,63]. As regards the first model, the thickness resulted to be 0.75 (+/- 0.01) nm. EAL was set at 0.48 nm for Si in the adlayer, as calculated from the NIST database [64]. 18 valence electrons were considered for the adlayer, the photoionization asymmetry parameter β was set at 1.03, and band gap was 2.5 eV. On the other hand, the thickogram graphical model resulted in SAM thickness equal to 0.80 nm (precision ~1%). S2s and Si2p peaks were identified as peculiar of the overlayer and the substrate zones, and data referring to ToA = 0° were considered. Relative sensitivity factors were 1.41 and 1.18 for sulfur and silicon, and the respective kinetic energies were 1258.6 and 1383.6 eV. Both thickness values obtained with EAL and thickogram models were slightly smaller than the theoretical length of MPTMS molecules, i.e., 0.9 nm [65], since the bonding of silane molecules to the surface required the loss of methoxy groups. Thus, the proposed synthesis protocol can precisely control the functionalization of the glass and confine it to a densely packed monolayer.

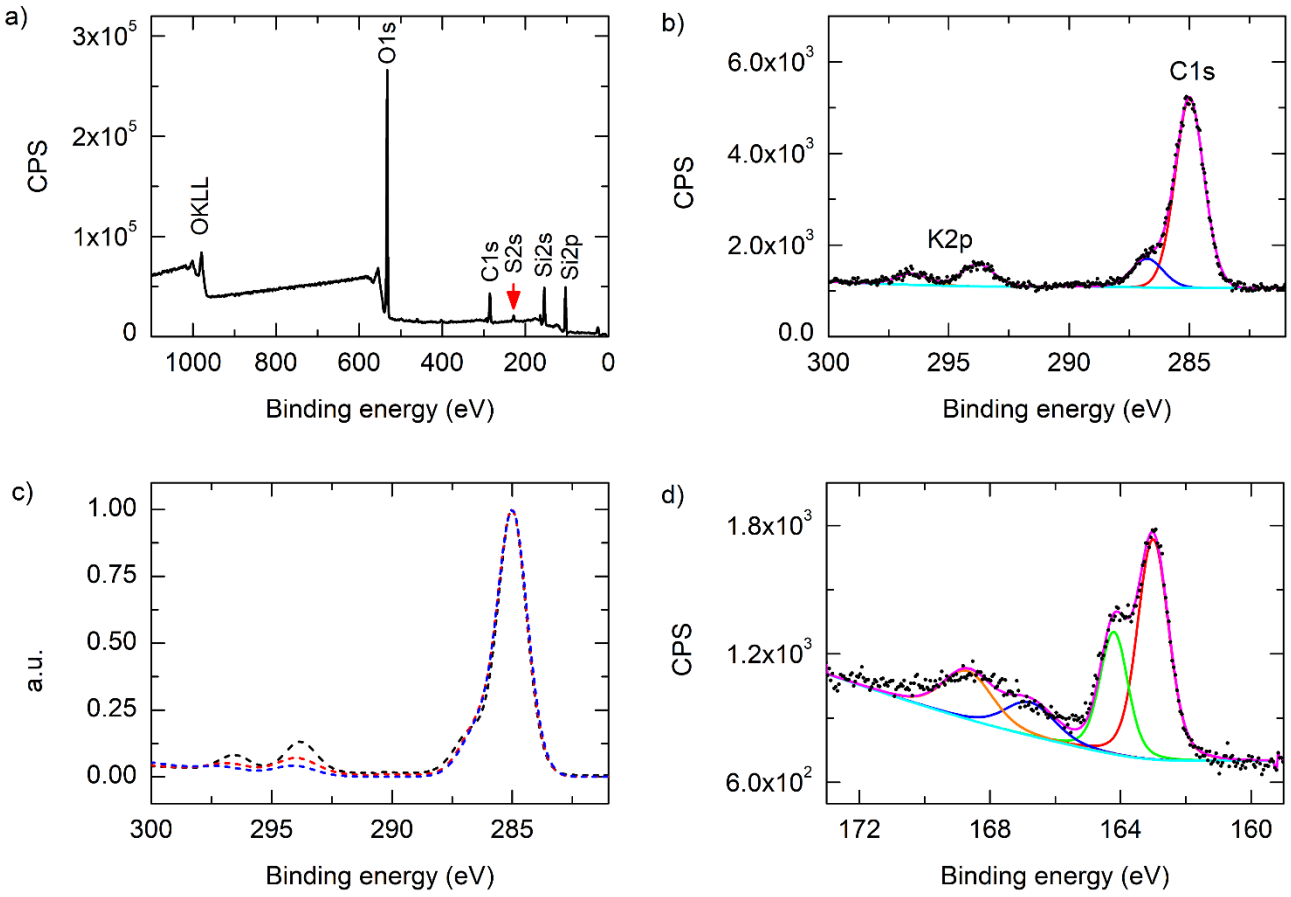

Figure 2. XPS survey of (a) thiol-functionalized glass at ToA = 0 °; (b) HR-XPS (ToA = 0°) of C1s peak and components fitting; (c) AR-HR-XPS of C1s normalized peaks at ToA = 0° (black), 45° (red) and 73° (blue); (d) HR-XPS (ToA = 0 °) of S2p peaks. All the HR-XPS fittings were performed with GL30 functions after U3 Tougaard background subtraction.

Topographies of bare and MPTMS functionalized glass were obtained from AFM and turned out to be essentially unaltered, as shown in Figure 3 (a) and (b). The average roughness was around 130 pm in both cases, pointing out that the surface modification occurred in a uniform fashion, without localized clusters of polymerized silane molecules or incomplete surface coverage by the organic layer. Furthermore, FE-SEM analyses of the metallized samples did not highlight any surface discontinuity. These results confirmed the suitability of the proposed synthesis protocol in leading to uniform superficial functionalization.

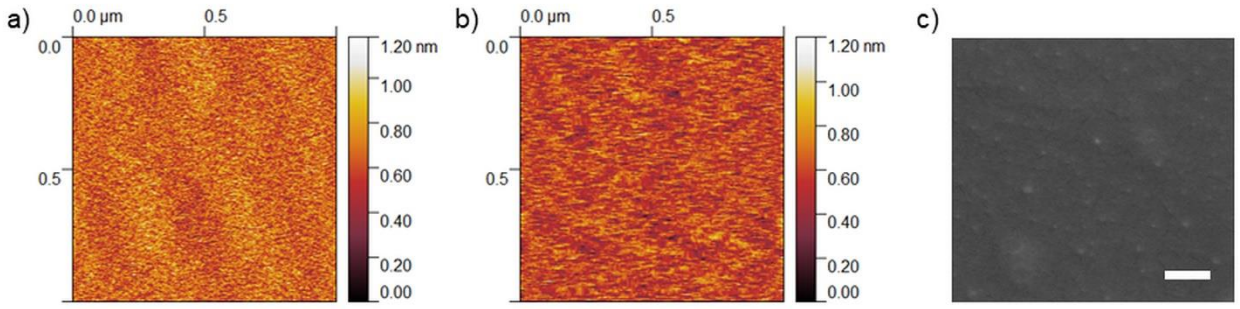

Figure 3. AFM topographies of (a) untreated and (b) thiol-functionalized glass. FE-SEM micrograph (c) of thiol-functionalized glass. Scale bar is 200 nm.

Once the optimal reaction medium was selected, the influence of two other process parameters on the synthesis outcome was investigated, namely the concentration of silane and the reaction temperature. As reported in Table 2, halving MPTMS amount in solution had a marginal impact on the contact angle and element ratios, whilst doubling the concentration led to higher contact angles and higher C/Si and S/Si ratios. The functionalization effectively occurred, as confirmed by the hydrophobic behavior of the surface, but C1s at% increased. This result likely related to the presence of surface islands of polymerized silanes, resulting from the excessive number of MPTMS molecules in solution. Thus, 0.054 M MPMTS was selected as the optimum since it led to the smaller standard deviations in at%, pointing out more uniform surface composition. A reservoir of silanes in solution is beneficial since the interaction with the surface is enhanced and bonding can be promoted before the decay of labile superficial hydroxylation. Lastly, higher contact angle values were obtained for the samples prepared heating the system at 40 °C for 4 h. The atomic composition showed major variations, S/C ratio being dramatically smaller. Moreover, HR-XPS of S2p region pointed out that 70% of the sulfur introduced on the surface was in the oxidized state, as reported in Figure S3. Reaction kinetics is enhanced by temperature but heating the system was found to be detrimental to the achievement of controlled synthesis conditions. The creation of disulfide bridges or other side reactions may have occurred between the sensitive thiol groups.

Successively, we used XPS to follow the reaction kinetics of MPTMS and APTMS. The relative concentrations of silicon, carbon and characteristic element of the adlayer (sulfur or nitrogen) as a function of

reaction time are reported in Figure 4. In both cases, the element characterizing the bulk of the sample, i.e., silicon, progressively decreases with time, whereas the elements peculiar to the adlayer, i.e., carbon and sulfur/nitrogen, showed an opposite trend. This was the result of the ongoing surface modification of the substrate by propane-thiol and propane-amino chains. However, despite the common general trend, a remarkable difference in the reaction kinetics of the two agents has been noticed. The coverage of glass surface by propane-thiol chains appeared to be slow and proceed smoothly, whereas propane-amino chains started to extensively bind to the surface in a shorter time, as proved by the sharp variation of chemical species in less than 1 h. The kinetics of assembly is known to be a 2-step process: diffusion-controlled adsorption and slow crystallization [1]. For thiol-SAM, the process turned out to be governed by the initial diffusion and anchoring of silanes to the active solid-liquid interface. The SAM formation was completed after 15 h, as all the concentrations reached a plateau. Conversely, amino-SAM formation was more difficult to control. Taking as reference the plateau values of Si2p, C1s and S2s concentrations of the previous case, the amino-SAM formation was achieved in less than 30 min. This reference could only be made as the two functionalizing molecules displayed exactly the same chemistry, except for one atom. Unlike thiol-SAMs, longer reaction times led to multilayering of the amino-silane over glass and thus were deleterious for the controlled functionalization of the surface. Finally, a plateau was reached, but the relative amount of carbon was more than three times higher than thiol-SAM. This result was corroborated by AFM analyses of excessively amino-functionalized glass, embedded in Figure 4 (b). The topography was found to be extremely irregular, with local deposits higher than 100 nm resulting from the uncontrolled polymerization of APTMS. These findings agreed with the ToF-SIMS analyses performed on the same samples. Spectra of the positive fragments were collected and then processed with NMF. Two endmembers were identified, one relative to the untreated glass and one representative of the last point of the kinetic curves. The scores showed the relationship of the endmembers with each sample and followed the same trend of XPS analyses, reported in Figure 4 (a) and (b).

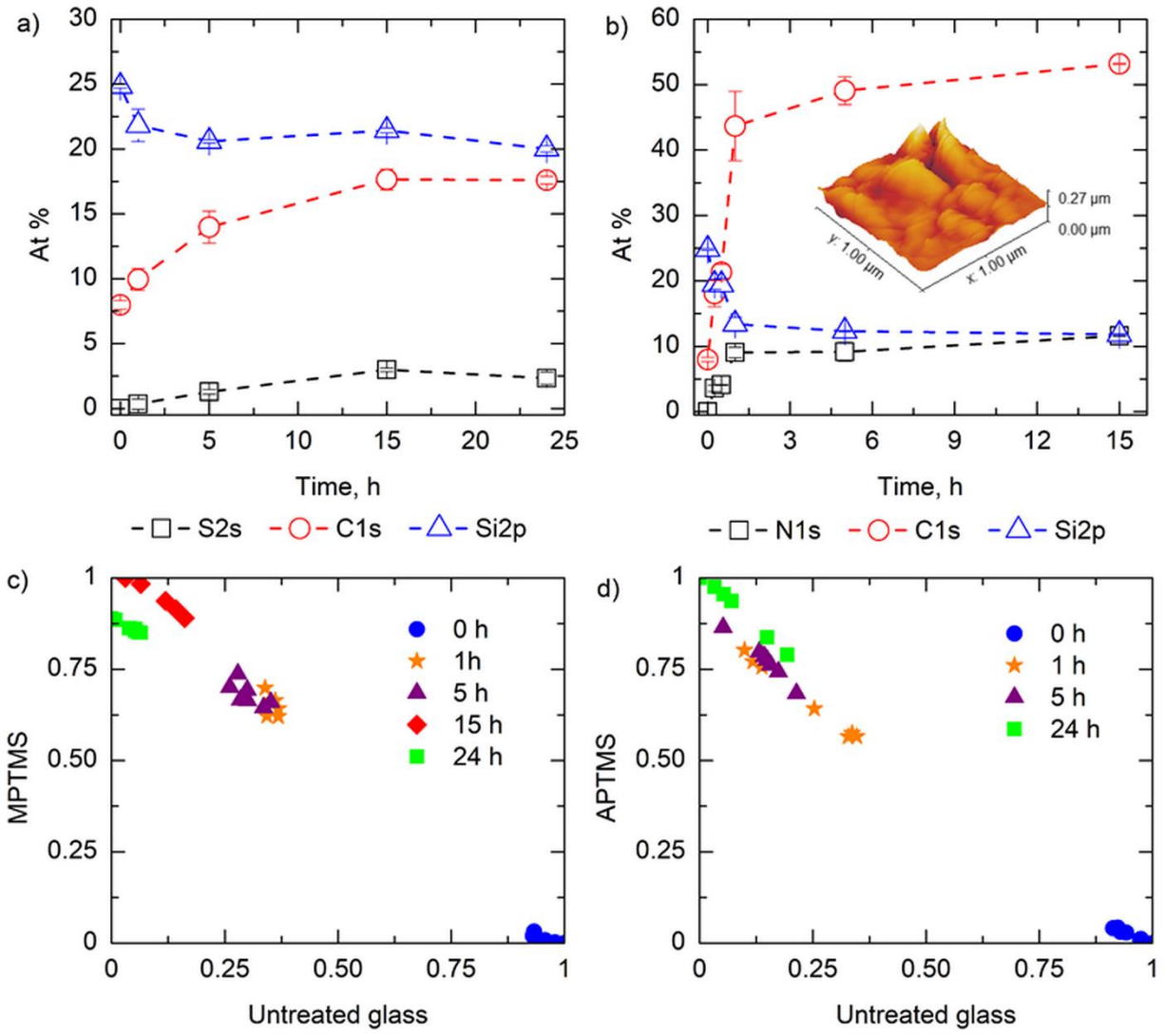

Figure 4. Kinetics of self-assembly of (a) thiol and (b) amino-terminated SAMs on pre-activated glass as evaluated from XPS survey scans. The relative concentrations of silicon, carbon, and sulfur or nitrogen are reported as a function of time. Embedded in panel (b) is the topography of an amino-functionalized glass prepared with a reaction time of 15 h, as measured with AFM. NMF analysis of ToF-SIMS spectra for (c) thiol and (d) amino-terminated SAMs synthesized with different reaction times.

The adjustment of the APTMS amount in solution for achieving control over the APTMS self-assembling process was also tested. All the samples were prepared keeping the reaction time at 15 h, while the concentration of silane was progressively reduced from 0.054 to 0.014 M. The samples were analyzed by XPS, see Table S5. As can be evinced, the manipulation of APTMS concentration was not efficient for gaining

control over the assembly process. The high C/Si ratio denoted an excess of carbon which was attributed to the presence of polymerized silane over the surface. Therefore, the reaction time turned out to be the key parameter for forcing the surface functionalization into a monolayer. More specifically, the optimal conditions were 0.054 M APTMS and 30 min as reaction time.

Two other silanes were considered to validate the synthesis protocol, namely 3-glycidyloxypropyltrimethoxysilane (GPTMS) and 3-(trimethoxysilyl)propylmethacrylate (TMSPM). Optimized synthesis involved concentration equal to 0.054 M and 15 h as reaction time for both silanes. Representative HR-XPS spectra of C1s regions are reported in Figure 5 to prove the effectiveness in anchoring the desired silanes. Details of relative at% of each component are reported in Table S6. In general, the C1s peak was fitted with the two components already discussed for MPTMS. However, significative differences linked to specific silane chemistry were highlighted. For APTMS SAMs, additional components relative to C=O and COO-H/R bonds at 288.0 eV and 288.9 eV were detected, indicating high sensitivity of the surface to external contamination. This aspect will be further discussed thanks to contact angle analyses. TMSPM SAMs displayed an intense COO-H/R component (about 9% of the C1s peak) attributed to the presence of methacrylate terminal groups. Finally, for GPTMS SAMs, the ratio between C-C (285.0 eV) and C-O (286.7 eV) components was around 0.6 because of the larger number of ether bonds coming from glycidyloxy terminal groups. Moreover, C-O and COO-H/R components were characterized by a slight binding energy shift compared to the previous samples (+0.1 eV and +0.2 eV respectively). In every case, K2p doublet was detected, suggesting that the functionalization occurred in thin layers.

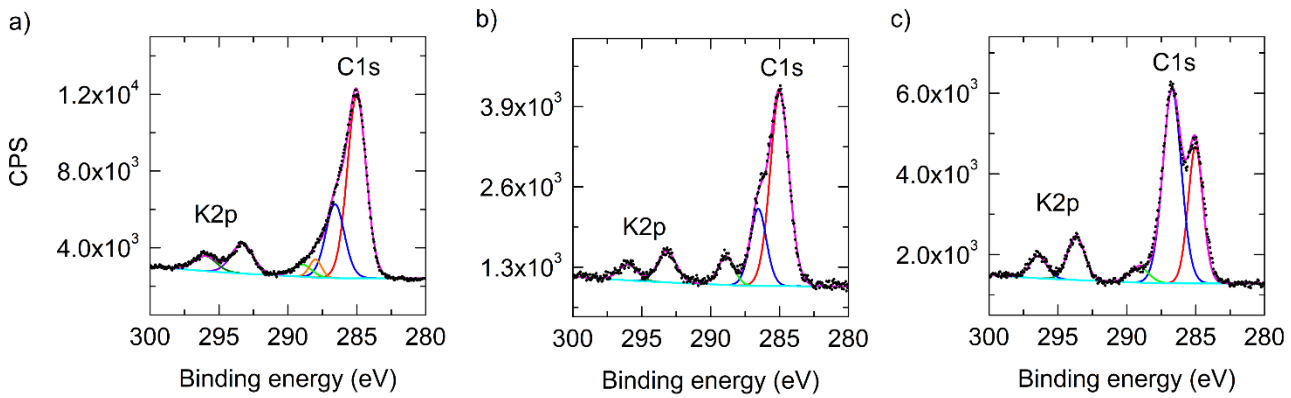

Figure 5. HR-XPS of C1s region of (a) amino, (b) methacrylate and (c) glycidyloxy-terminated SAMs recorded at ToA = 0°. Peak components are detailed in Table S6.

To confirm the hypothesis of a thin functionalized layer, the ellipsometry technique was selected. The results concerning the calculated SAMs thicknesses and refractive indexes (n_{SAM}) are collected in Table 3. The height of organic layer turned out to be congruent with the theoretical molecule length, being around 1 nm for all the silanes. As regards MPTMS SAM, the thickness values obtained by ellipsometry (0.75 nm) were in good agreement with those obtained by XPS (0.80 nm). Such an evidence further corroborated the effective monolayer formation.

Table 3. Refractive indexes of silanes and adlayer, SAM thickness and packing factors as calculated from ellipsometry.

Sample	**Thickness, nm**	n_{SAM}, -	n_{mol}, -	f_{mol}, %
MPTMS	0.75	1.443	1.444	99.8
APTMS	0.76	1.429	1.424	100
TMSPM	0.83	1.350	1.431	81.2
GPTMS	0.90	1.423	1.429	98.6

The refractive index of the adlayer, n_{SAM}, was evaluated in order to calculate the packing factor of the organic layer, f_{mol}:

$$f_{mol} = \frac{n_{SAM} - n_{air}}{n_{mol} - n_{air}} \quad (1)$$

Knowing the refractive indexes of air, n_{air} = 1.00027, and silane molecules, n_{mol} as declared by the chemicals' manufacturer, one can estimate and compare the packing behavior of different functionalizing agents. The silanes having terminal groups with limited steric hindrance displayed the highest degree of packing, equal to

99.8 and 100% for thiol and amino groups, respectively. f_{mol} slightly decreased for GPTMS SAM, whereas it dropped for TMSPM ones. This result was attributed to the conformation of the silane molecules, ranging from "slim" thiol and amino groups, to bolder epoxy and methacrylate substituents. Lastly, f_{mol} was also calculated for selected samples of the MPMTS kinetics of assembly study. The packing factor progressively increased when approaching the plateau conditions: at t = 1 h, f_{mol} was equal to 67%, whereas it reached almost 100% after 15 h of silanization time.

Table 4 illustrates the results obtained from static contact angle and surface zeta potential measurements of the reference samples for each surface chemistry considered in this study. The contact angle values reported in literature are quite polydisperse as regards silane-based SAMs [66,67]. As a general trend, the introduction of a propylic chain bearing some terminal groups increased the hydrophobicity of the surface, the contact angle being higher than 60° for most of the samples. A different behavior was noticed for the amino-SAM, whose contact angle was significantly smaller, i.e., around 34°. This was attributed to the tendency to protonation of the amino exposed groups in presence of water [68]. However, it has to be underlined that this result was observed only when performing the measurement immediately after the synthesis. The contact angle would increase already after 10 hours, reaching values higher than 80° after a week. The electrostatic forces acting on the SAM were believed to be responsible for this behavior. In fact, among all the analyzed samples, only amino-SAMs had a positive surface zeta potential (Table 4). As a consequence of the positive charges on the surface, the adsorption of impurity particles from the atmosphere, which are usually negatively charged, would be enhanced. This may result in the alteration of the SAM chemistry and morphology, leading to an out-of-specs surface. All the other SAMs displayed a negative or neutral surface zeta potential and a stable contact angle value over time.

Table 4. Water contact angle, surface zeta potential and relative standard deviations of untreated glass and SAMs carrying different head groups.

Sample	***Contact angle, °***	***Std dev, °***	***SZP, mV***	***Std dev, mV***

Untreated glass	62.9	5.4	-14.6	3.9
MPTMS	65.7	1.7	- 42.3	2.1
APTMS	33.8	2.6	+ 14.9	4.9
TMSPM	65.4	1.7	- 21.3	2.5
GPTMS	62.8	1.5	-24.7	3.9

Finally, ToF-SIMS analyses of untreated and MPMTS, APTMS and TMSPM functionalized glass were performed. For this part of the study, all the samples were prepared with 0.054 M silane in anhydrous toluene at room temperature for 15 h. Representative spectra of positive fragments are reported in Figure S4, whereas the results emerged from NMF and PCA analyses of ToF-SIMS data are shown in Figure 6. Because of the NMF processing, spectra relative to the same sample were successfully grouped and separated. The alteration of surface chemistry in an identifiable manner was demonstrated as surface chemistries were successfully isolated in the endmember space by NMF. Moreover, by performing PCA on the samples' spectra, the components responsible for the larger differences between samples were isolated. As can be seen in Figure 6 (b), the characteristic fragments were those involving mainly carbon, sulfur and nitrogen. The characteristic elements were present in fragments involving carbon since cationization had extracted them as bound to a hydrocarbon tail. As a general trend, the most intense peaks of untreated glass were related to short hydrocarbon chains ($C \leq 6$), attributable to surface contamination. For MPMTS, APTMS and TMSPM, shorter hydrocarbon fragments were the most significant ones, with a predominance of light hydrocarbon fragments, as expected considering the presence of propylic chains on the surface.

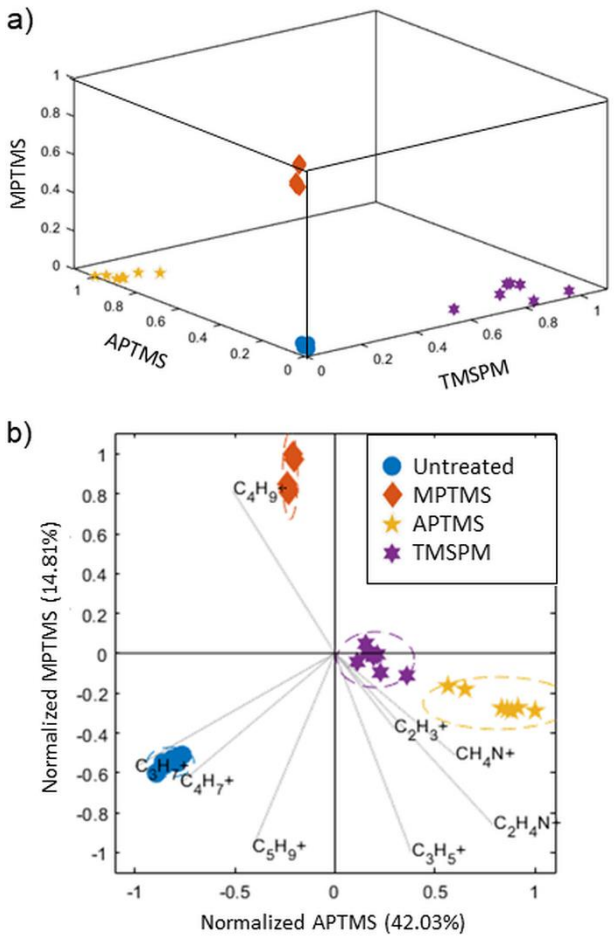

505

Figure 6. (a) NMF and (b) PCA analyses of ToF-SIMS positive spectra of untreated glass, MPTMS, APTMS, and TMSPM functionalized glass. All the samples were prepared with 0.054 M silane in anhydrous toluene and reaction time = 15 h.

510 Our SAMs were designed to tackle the crystallization of biomolecules and drugs and, in particular, their nucleation step. As proof of concept, the crystallization of a small molecule drug, namely aspirin (ASA), is here presented. The cumulative probability of observing nucleation events on untreated glass, thiol, and amino SAMs is sketched in Figure 7. The presence of surfaces carrying different functionalizations strongly affected the time needed to observe the first crystals. Compared to untreated glass, which was taken as a blank,
515 amino SAMs had a strong promotion effect over ASA crystallization. Conversely, thiol SAMs were found to act as nucleation inhibitors. Both SAMs halved the time elapsed between the setting of the experiment and the

onset of nucleation, compared to the blank. However, amino SAMs boosted nucleation and led to 100% probability of finding crystals in each crystallizer. Thiol SAMs, on the contrary, strongly inhibited the nucleation step, decreasing the cumulative probability to 30%. Therefore, the ability of the presented SAMs in affecting the nucleation of pharmaceuticals was demonstrated.

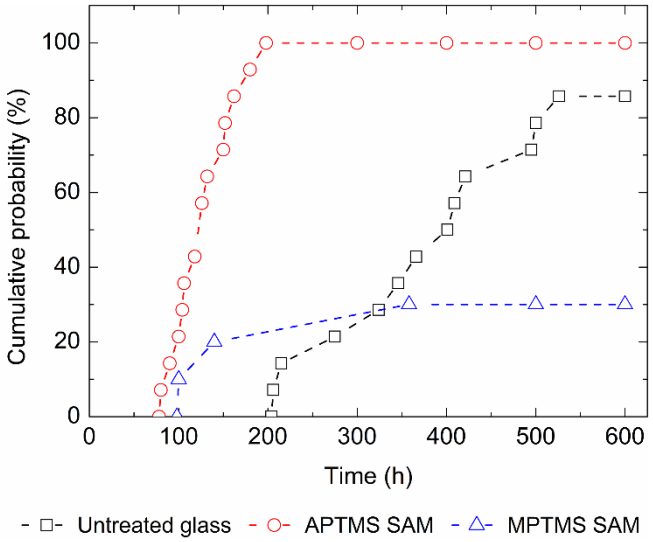

Figure 7. The cumulative probability of finding ASA crystals on untreated glass, APTMS and MPTMS SAMs as a function of time.

Conclusion

In this paper, the development and optimization of a single protocol for the synthesis of four high-quality SAMs was presented. The control of the functionalization step of pre-activated glass was achieved by tuning synthesis parameters such as reaction medium, silane concentration, reaction time, and temperature. The optimal set of process conditions was found to be dependent on the silane terminal group, with reaction time being the most affected parameter. In this scenario, the kinetics of self-assembly of thiol and amino-terminated silanes was deeply investigated. XPS and ToF-SIMS pointed out the same temporal evolution of surface chemistry modification. The monolayer conditions were achieved in 15 h and 30 min for thiol and amino-terminated silanes, respectively. Moreover, High Resolution and Angle-Resolved XPS confirmed the expected chemical state of the elements and the extremely thin layer introduced by the surface modification. For

example, the thickness of the MPMTS SAM was 0.8 nm, as calculated by XPS and confirmed by ellipsometry. The surface functionalization involved a single layer of silane molecules. The proposed synthesis protocol enabled the creation of SAMs exposing different functional groups on glass, thus tailoring its wettability and electrostatic properties without altering its topography. Since the superficially exposed chemistry is the only variable among the samples, our SAMs represent an ideal platform for probing the molecular interactions between surfaces and molecules in solution during a crystallization process. SAMs could effectively control the nucleation kinetics of aspirin, acting as promoters or inhibitors. As a step further, the controlled crystallization of proteins on SAMs will be presented in an upcoming study.

Abbreviations

AFM, Atomic Force Microscopy; APTMS, 3-aminopropyltrimethoxysilane; AR, Angle-Resolved; ASA, aspirin; ATR, Attenuated Total Reflectance; DLS, Dynamic Light Scattering; EAL, Electronic Attenuation Length; FE-SEM, Field Emission Scanning Electron Microscopy; FT-IR, Fourier Transformed InfraRed; GPTMS, 3-glycidyloxypropyltrimethoxysilane; HR, High Resolution; LMIG, Liquid Metal Ion Gun; MPTMS, 3-mercaptopropyltrimethoxysilane; MSE, Mean Square Error; MVA, Multi Variate Analysis; NMF, Non-negative Matrix Factorialization; PCA, Principal Component Analysis; SAD, Selected Area Difference; SAM, Self-Assembled Monolayer; Std Dev, Standard Deviation; SZP, Surface Zeta Potential; ToA, Take-off Angle; ToF SIMS, Time-of-Flight Secondary Ion Mass Spectrometry; TMSPM, 3-(trimethoxysilyl)propylmethacrylate; XPS, X-Ray Photoelectron Spectroscopy;

Nomenclature

f_{mol}, packing factor; n_{air}, air refractive index; n_{mol}, molecule refractive index; n_{SAM}, SAM refractive index; R_q, surface roughness.

Acknowledgements

The results reported in this study were obtained thanks to the access to the Nanobiotechnology Laboratory under the Framework for Open Access to the Joint Research Centre Research Infrastructures of the European Commission (agreement n° 35194/10).

Bibliography

[1] G.M. Whitesides, B. Grzybowski, Science **295**, 2418 (2002).

[2] L. Passoni, L. Criante, F. Fumagalli, F. Scotognella, G. Lanzani, F. Di Fonzo, ACS Nano **8**, 12167 (2014).

[3] T. Wink, S.J. Van Zuilen, A. Bult, W.P. Van Bennekom, Analyst. **122**, 43 (1997).

[4] V. Spampinato, M.A. Parracino, R. La Spina, F. Rossi, G. Ceccone, Front. Chem. **4**, (2016).

[5] F. Artusio, R. Pisano, Int. J. Pharm. **547**, 190 (2018).

[6] D. Ji, C.M. Arnold, M. Graupe, E. Beadle, R. V. Dunn, M.N. Phan, R.J. Villazana, R. Benson, R. Colorado, T. Randall Lee, J.M. Friedman, J. Cryst. Growth **218**, 390 (2000).

[7] P. Marmont, N. Battaglini, P. Lang, G. Horowitz, J. Hwang, A. Kahn, C. Amato, P. Calas, Org. Electron. **9**, 419 (2008).

[8] D. Liu, Q. Miao, Mater. Chem. Front. **2**, 11 (2018).

[9] Z. Yan, Z. Sun, W. Lu, J. Yao, Y. Zhu, J.M. Tour, ACS Nano **5**, 1535 (2011).

[10] J. Osicka, M. Ilčiková, A. Popelka, J. Filip, T. Bertok, J. Tkac, P. Kasak, Langmuir **32**, 5491 (2016).

[11] L. Jian, J. Exp. Nanosci. **3**, 307 (2008).

[12] C. Rodriguez, A.M. Noval, V. Torres-Costa, G. Ceccone, M.M. Silván, Materials (Basel) **12** (2019).

[13] V. Chechik, R.M. Crooks, C.J.M. Stirling, Adv. Mater. **12**, 1161 (2000).

[14] W. Senaratne, L. Andruzzi, C.K. Ober, Biomacromolecules **6**, 2427 (2005).

[15] E. Ruckenstein, Z.F. Li, Adv. Colloid Interface Sci. **113**, 43 (2005).

[16] F. Artusio, M. Bazzano, R. Pisano, P.E. Coulon, G. Rizza, T. Schiller, M. Sangermano, Polym. (United Kingdom) **139**, 155 (2018).

[17] F. Artusio, A. Ferri, V. Gigante, D. Massella, I. Mazzarino, M. Sangermano, A. Barresi, R. Pisano, Drug Dev. Ind. Pharm. **45**, 1862 (2019).

[18] M. Beiner, G.T. Rengarajan, S. Pankaj, D. Enke, M. Steinhart, Nano Lett. **7**, 1381 (2007).

[19] E.N. Athanasopoulou, N. Nianias, Q.K. Ong, F. Stellacci, Nanoscale **10**, 23027 (2018).

[20] J. Fick, R. Steitz, V. Leiner, S. Tokumitsu, M. Himmelhaus, M. Grunze, Langmuir **20**, 3848 (2004).

[21] B.C. Dallin, H. Yeon, A.R. Ostwalt, N.L. Abbott, R.C. Van Lehn, Langmuir **35**, 2078 (2019).

[22] A.K. Chew, R.C. Van Lehn, J. Phys. Chem. C. **122**, 26288 (2018).

[23] E. Finocchio, E. Macis, R. Raiteri, G. Busca, Langmuir **23**, 2505 (2007).

[24] E. Pavlovic, A.P. Quist, U. Gelius, S. Oscarsson, J. Colloid Interface Sci. **254**, 200 (2002).

[25] P. Pallavicini, G. Dacarro, M. Galli, M. Patrini, J. Colloid Interface Sci. **332**, 432 (2009).

[26] N.R. Glass, R. Tjeung, P. Chan, L.Y. Yeo, J.R. Friend, Biomicrofluidics **5** (2011).

[27] Y. Yang, A.M. Bittner, S. Baldelli, K. Kern, Thin Solid Films **516**, 3948 (2008).

[28] G.A. Husseini, J. Peacock, A. Sathyapalan, L.W. Zilch, M.C. Asplund, E.T. Sevy, M.R. Linford, Langmuir **19**, 5169 (2003).

[29] A. Ulman, Chem. Rev. **96**, 1533 (1996).

[30] B.C. Bunker, R.W. Carpick, R.A. Assink, M.L. Thomas, M.G. Hankins, J.A. Voigt, D. Sipola, M.P. De Boer, G.L. Gulley, Langmuir **16**, 7742 (2000).

[31] K.T. Tan, C.C. White, D.L. Hunston, C. Clerici, K.L. Steffens, J. Goldman, B.D. Vogt, J. Adhes. **84**, 339 (2008).

[32] M. Hu, S. Noda, T. Okubo, Y. Yamaguchi, H. Komiyama, Appl. Surf. Sci. **181**, 307 (2001).

[33] R. La Spina, V. Spampinato, D. Gilliland, I. Ojea-Jimenez, G. Ceccone, Biointerphases **12**, 031003 (2017).

[34] J.W. Park, J.S. Shumaker-Parry, ACS Nano **9**, 1665 (2015).

[35] B. Oberleitner, A. Dellinger, M. Déforet, A. Galtayries, A.S. Castanet, V. Semetey, Chem. Commun. **49**, 1615 (2013).

[36] D. Samanta, A. Sarkar, Chem. Soc. Rev. **40**, 2567 (2011).

[37] A. Taglietti, G. Dacarro, D. Barbieri, L. Cucca, P. Grisoli, M. Patrini, C.R. Arciola, P. Pallavicini, Materials (Basel) **12** (2019).

[38] C. Haensch, S. Hoeppener, U.S. Schubert, Chem. Soc. Rev. **39**, 2323 (2010).

[39] S. Casalini, C.A. Bortolotti, F. Leonardi, F. Biscarini, Chem. Soc. Rev. **46**, 40 (2017).

[40] G.C. Allen, F. Sorbello, C. Altavilla, A. Castorina, E. Ciliberto, Thin Solid Films **483**, 306 (2005).

[41] P.M. Dietrich, C. Streeck, S. Glamsch, C. Ehlert, A. Lippitz, A. Nutsch, N. Kulak, B. Beckhoff, W.E.S. Unger, Anal. Chem. **87**, 10117 (2015).

[42] C.R. Kessel, S. Granick, Langmuir **7**, 532 (1991).

[43] C.T. Buscher, D. McBranch, D.Q. Li, J. Am. Chem. Soc. **118**, 2950 (1996).

[44] M. Wang, K.M. Liechti, Q. Wang, J.M. White, Langmuir **21**, 1848 (2005).

[45] C.H. Kuo, H.Y. Chang, C.P. Liu, S.H. Lee, Y.W. You, J.J. Shyue, Phys. Chem. Chem. Phys. **13**, 3649 (2011).

[46] H.G. Tompkins, W.A. McGahan, *Spectroscopic Ellipsometry and Reflectometry: A User's Guide* (John Wiley & Sons, Inc., New York, 1999).

[47] S. Tougaard, Surf. Interface Anal. **26**, 249 (1998).

[48] S. Tougaard, F. Yubero, Surf. Interface Anal. **36**, 824 (2004).

[49] B.J. Tyler, G. Rayal, D.G. Castner, Biomaterials **28**, 2412 (2007).

[50] D.J. Graham, D.G. Castner, Biointerphases **7** (2012).

[51] G.F. Trindade, M.L. Abel, J.F. Watts, Chemom. Intell. Lab. Syst. **163**, 76 (2017).

[52] G.F. Trindade, M.L. Abel, J.F. Watts, Chemom. Intell. Lab. Syst. **182**, 180 (2018).

[53] A. Henderson, *TOF-SIMS: Materials Analysis by Mass Spectrometry* (Surface Spectra, UK, 2013) pp. 449-484.

[54] See: J. Shlens, A Tutorial on Principal Component Analysis, http://arxiv.org/abs/1404.1100 (2014).

[55] G. Beamson, D. Briggs, *XPS of Polymers Database* (Surface Spectra, UK, 1992).

[56] S. Onclin, B.J. Ravoo, D.N. Reinhoudt, Angew. Chemie - Int. Ed. **44**, 6282 (2005).

[57] N. Herzer, S. Hoeppener, U.S. Schubert, Chem. Commun. **46**, 5634 (2010).

[58] M.J.P. Roldán, C.P. García, G. Marchesini, D. Gilliland, G. Ceccone, D. Mehn, P. Colpo, F. Rossi, Microelectron. Eng. **88**, 1948 (2011).

[59] F. Schreiber, Prog. Surf. Sci. **65**, 151 (2000).

[60] M. Dhayal, D.M. Ratner, Langmuir **25**, 2181 (2009).

[61] F. Cheng, L.J. Gamble, D.G. Castner, Anal. Chem. **80**, 2564 (2008).

[62] C.D. Bain, G.M. Whitesides, J. Phys. Chem. **93**, 1670 (1989).

[63] P.J. Cumpson, P.C. Zalm, Surf. Interface Anal. **29**, 403 (2000).

[64] C.J. Powell, A. Jablonski, J. Surf. Anal. **9**, 322 (2002).

[65] M. Ben Ali, F. Bessueille, J.M. Chovelon, A. Abdelghani, N. Jaffrezic-Renault, M.A. Maaref, C. Martelet, Mater. Sci. Eng. C **28**, 628 (2008).

[66] N.H. Nordin, Z. Ahmad, J. Phys. Sci. **26**, 11 (2015).

[67] D.F.S. Petri, G. Wenz, P. Schunk, T. Schimmel, Langmuir **15**, 4520 (1999).

[68] H. Zhang, H.X. He, J. Wang, T. Mu, Z.F. Liu, Appl. Phys. A Mater. Sci. Process. **66**, 269 (1998).

Graphical abstract